Available online at www.sciencedirect.com
ScienceDirect
Journal of Power Sources 160 (2006) 359–373
JOURNAL OF POWER SOURCES
www.elsevier.com/locate/jpowsour

Parameter sensitivity examination and discussion of PEM fuel cell simulation model validation
Part I. Current status of modeling research and model development

W.Q. Tao *, C.H. Min, X.L. Liu, Y.L. He, B.H. Yin, W. Jiang

State Key Laboratory of Multiphase Flow in Power Engineering, School of Energy and Power Engineering, Xi'an Jiaotong University, Xi'an, Shanxi 710049, PR China

Received 17 December 2005; received in revised form 12 January 2006; accepted 25 January 2006
Available online 9 March 2006

Abstract

Mathematical modeling plays an important role in fuel cell design. A comprehensive review of the mathematical modeling of proton exchange membrane fuel cells is first conducted. It is found that the results computed by different models in the literature often agree well with the experimental data. This stimulates the present authors to carry out a comprehensive parameter sensitivity examination. In this first paper a three-dimensional, two-phase and non-isothermal model is developed, and numerical simulations for a basic case is performed, the results of which are regarded as the reference for further sensitivity examination. All the parameters needed for the simulation are provided in detail. In the companion paper (Part II), the results of the parameter sensitivity analyses and discussion of model validation are provided in detail.

Keywords: PEM fuel cell; Parametric sensitivity; Model; Polarization curve

1. Introduction

The proton exchange membrane fuel cell (PEMFC) is considered to be a promising power source, especially for transportation and stationary cogeneration applications due to its high efficiency, low-temperature operation, high power density, fast start-up, and system robustness. In the last decade a great number of researches have been conducted to improve the performance of the PEMFC, so that it can reach a significant market penetration. Ref. [1–5] are the examples of very recent publications. In this regard, an optimization study of the PEMFC plays an important role. One of the important tools in the optimization study of fuel cell performance is computational modeling, which can be used to reveal the fundamental phenomena taking place in the fuel cell system, predict fuel cell performance under different operating conditions, reveal the distribution details of various dependent variables and optimize the design of a fuel cell system [6].

The processes in the fuel cells are very complicated because of the very tight coupling between electrochemical and transport processes. For modeling of a single fuel cell, the parameters of electrochemical kinetics, fluid flow, mass transfer, heat transfer and species transfer are included. Because the number of the flow channels in the bipolar plate is quite large, and there are seven functional regions across the fuel cell, with the present-day models available to most researchers are often impossible to use to numerically simulate the whole fuel cell. Therefore, a typical element is usually separated from the whole fuel cell in the computational domain. Although this element only covers part of the fuel cell, it includes all functional parts of the fuel cell: from the anode channel to the cathode channel. Thus, based on the assumption that the process is periodic from channel to channel, such an element may be regarded as the representation of the entire fuel cell. This kind of numerical simulation may be called a typical unit simulation of a single fuel cell. The work reviewed and presented in this paper belongs to this category of simulation.

Because of the complexity of the process, there are more than ten empirical or experimental parameters involved in the physical modeling of the PEMFC. To validate the physical and

DOI of original article:10.1016/j.jpowsour.2006.01.080.
* Corresponding author. Tel.: +86 29 82669106; fax: +86 29 82669106.
E-mail address: wqtao@mail.xjtu.edu.cn (W.Q. Tao).

0378-7753/$ – see front matter © 2006 Elsevier B.V. All rights reserved.
doi:10.1016/j.jpowsour.2006.01.078

Nomenclature

a	water activity
A	area (m^2)
A_s	specific area of catalyst layer (m^{-1})
c	molar concentration ($mol\,m^{-3}$)
D	diffusion coefficient ($m^2\,s^{-1}$)
F	Faraday's constant ($C\,mol^{-1}$)
h_m	evaporation and condensation rate
H	height (m)
i	reaction rate ($A\,m^{-3}$)
i_{ref}	reference exchange current density ($A\,m^{-2}$)
I	current density ($A\,m^{-2}$)
k	thermal conductivity ($W\,m^{-1}\,K^{-1}$)
K	electrode absolute permeability (m^2)
L	length (m)
M	molar mass ($kg\,mol^{-1}$)
n	electron number of electrochemical reaction
p	pressure (Pa)
R	universal gas constant ($8.314\,J\,mol^{-1}\,K^{-1}$)
s	liquid water saturation
S	source term of governing equations
T	temperature (K)
$\mathbf{u}$	velocity vector ($m\,s^{-1}$)
V	potential (V)
w	velocity at z-direction ($m\,s^{-1}$)
W	width (m)
x, y, z	coordinate (m)
X	species mass fraction (dimensionless)

Greek symbols

α	transfer coefficient
ε	porosity
ζ	stoichiometric flow ratio
η	overpotential (V)
κ	electrical conductivity ($S\,m^{-1}$)
λ	membrane water content
μ	viscosity ($kg\,m^{-1}\,s^{-1}$)
ν	kinetic viscosity ($m^2\,s^{-1}$)
ρ	density ($kg\,m^{-3}$)
σ	surface tension ($N\,m^{-1}$)
ϕ	potential (V)
ω	species molar fraction

Subscripts and superscripts

a	anode
av	average value
c	cathode
cc	land area
ch	channel
ct	catalyst layer
d	diffusion layer
eff	effective
g	gas
h	hydrogen
in	inlet
k	species
l	liquid
m	membrane
o	oxygen
oc	open circuit
r	relative values
ref	reference values
s	solid; specific
sat	saturation
tot	total
w	water

numerical models, comparison with some experimental data is highly desirable. For the fuel cell performance description, the polarization curve, or voltage-current curve, is one of the most important final outcomes of numerical simulation. For a comparison with experimental results, the most widely cited test data of the polarization curve in previous literature are the ones presented by Ticianelli et al. in [7,8]. By careful review of the existing literature available to the present authors, it was found that different models with different parameters were adopted in simulations, while the final outcome, i.e., the curves for the fuel cell voltage versus current were often almost the same. What was more interesting was the fact that the comparison of different simulation results with the same test data [7,8] often showed good agreement. This situation stimulates the present authors to conduct a parameter sensitivity examination for two purposes: Firstly, to reveal what parameters have the most significant effects on the *V–I* curve; secondly, to examine whether the comparison with test data of the *V–I* curve is enough to validate a model.

This paper is the first part of a two-part study on the parameter sensitivity study and a discussion of the validation model. The rest of the paper is organized as follows. In order to have a clear understanding of the above-mentioned situation, a comprehensive review of numerical models will first be conducted. Then, a three-dimensional two-phase and non-isothermal model will be presented for the parameter sensitivity study. Numerical methods, a solution flow-chart and grid-independence examination for the proposed model will be presented. The numerical simulation results for a basic case will be shown which as the reference for a further parameter sensitivity examination. Finally some conclusions will be made. The results of the parameter sensitivity study and a detailed discussion of the model validation will be presented in the companion paper.

2. Review of existing PEM fuel cell models

The schematic of a PEMFC is shown in Fig. 1. The anode gas channel (in a bipolar plate), the anode diffusion layer, the anode catalyst layer, the ion-conducting membrane, the cathode catalyst layer, the cathode diffusion layer, and the cathode gas channel are components of the PEMFC. Bipolar plates act as electron collectors. Anode gas channels supply the fuel cell

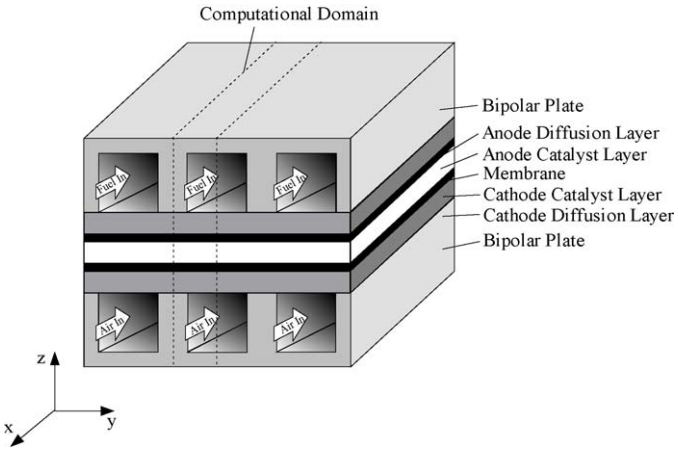

Fig. 1. Schematic view of a PEMFC.

with reactants, which are transported by convection and diffusion throughout the anode gas channel. The electronically conducting porous diffusion layers allow for more or less even distribution of the reactants over the anode and cathode. Hydrogen oxidation and oxygen reduction reactions are considered to occur only within the anode catalyst layers and cathode catalyst layers, respectively. The catalyst layers also provide channels for transfer of electrons and protons. The ion-conducting membrane spatially separates the fuel cell into two parts and only allows the transport of water and protons.

2.1. Classification of the PEMFC simulation models

A number of simulation models have been developed. These models can generally be characterized by the computational scope of the model. One kind of model focuses on a specific part or parts of the fuel cells [9], such as the cathode catalyst layer [10–14], the electrode [15–18], the gas diffusion layer [19], the membrane electrode assembly [20,21], or the ion-conducting membrane [22–24]. Ref. [25] reviewed the Nafion membrane structure and properties. These models are useful. However, they cannot provide a complete picture of the fuel cell. The other kinds of models include all parts of a fuel cell, from one-dimensional and single-phase to three-dimensional and two-phase.

The most prominent earlier work was from Bernardi and Verbrugge [21,26,27] and Springer et al. [20,28], who developed one-dimensional models. Later, Eikerling et al. [29], Baschuk and Li [30], Rowe and Li [31] and Maggio et al. [32] developed other one-dimensional models. These models can predict the cell *V–I* performance in the low and intermediate current density ranges with reasonably good agreement of the test data, but fail to reproduce the concentration polarization in the polarization region [33]. Therefore, two-dimensional models were presented by: Kulikovsky et al. [11], Nguyen and White [34], Yi and Nguyen [35], Gurau et al. [36], Kazim et al. [37], Singh et al. [38], He et al. [39], Wang et al. [40], Natarajan and Nguyen [41] and Hsing and Futerko [42]. A relatively simpler approach to model the plane formed by the direction across the fuel cell and the direction along the flow channel is called a quasi-two-dimensional model [43,44]. In these models, a one-dimensional model for one direction is coupled with another one-dimensional model for another direction normal to the previous one to simulate the profiles in the plane. The two-dimensional models can only simulate the plane perpendicular to the flow channels (in *z–y* plane of Fig. 1) or the plane formed by the direction across the fuel cell and the direction along the flow channel (*z–x* plane of Fig. 1). Therefore, these models cannot give a full picture of the variations in the temperature and reactants in a typical three-dimensional element. In order to have a better understanding of how the actual fuel cell performs, it is necessary to have a three-dimensional model. Three-dimensional models are being developed. Dutta et al. [45,46], Shimpalee and Dutta [47], Berning et al. [48], Berning and Djilali [49], Jen et al. [50], Li et al. [51], Hu et al. [52], Um and Wang [53], Nguyen et al. [54], Zhou and Liu [55] and Ju et al. [56] have all presented three-dimensional models. Like the quasi-two-dimensional model, some quasi-three-dimensional models are developed in [57,58].

2.2. Validation issues for PEM fuel cell models

As indicated above, modeling research on the PEM fuel cell is being developed quickly. As indicated in [59] all models should be validated by experimental data such as presented in [7,8] or by other successful models [60]. From the literature, most of the models are validated by experimental data. The general method used is the polarization curve, i.e., *V–I* curve computed by the model is compared with the polarization curve measured by experiment. If two *V–I* curves are in good agreement, the model is usually considered reliable. There are two methods of comparison with test data. In one, the authors who developed the model measured the experimental data themselves [8,31,56,61–66] or together with other research groups [67]. However, most authors take the other route: validating their models by comparing their numerical results with the experimental data published by other research groups [10,30,52,60,67–79]. Our discussion is focused on the second method. We have found that often the results computed by different models agree surprisingly well with the same experimental data. It should be noted that many empirical parameters involved in different models are often very different or even rather different from the experimental data used for validation of the model. For example, we find that there are at least fourteen papers which used the experimental data published by Ticianelli et al. [7,8] to validate their models. These include following papers: the one-dimensional single-phase model of [26,60,80], two-dimensional single-phase models of [35,37,81–83], three-dimensional single-phase models of [47,49,81,82,84] and three-dimensional two-phase models of [85–87]. We find that [7,8] did not supply all of the parameters the models need. These two papers supplied many polarization curves under different conditions. Many papers used the same curve under conditions corresponding to the following case: polymer–electrolyte, 20 wt.% Pt, 50-nm sputtered Pt, 5 atm cathode pressure, 3 atm anode pressure and a 353 K cell temperature. Some representative parameters used in ten papers are listed in Table 1, which shows that most of the parameters used in the ten papers are different from each other, but the *V–I* curves of the

Table 1
Parameters used in 10 papers

	Unit	[26]	[35]	[81,82]	[83]	[48]	[84]	[85,86]	[87]
L	m		0.0762	0.07112	0.07112	0.0767	0.01067	0.0711	0.05
W	m					7.62×10^{-4}		1.0×10^{-3}	1.0×10^{-3}
W_{cc}	m							1.0×10^{-3}	1.0×10^{-3}
H_{ch}	m		7.62×10^{-4}	7.62×10^{-4}	7.62×10^{-4}	5.0×10^{-3}	7.62×10^{-4}	7.62×10^{-4}	1.0×10^{-3}
H_d	m	2.6×10^{-4}	2.54×10^{-4}	2.54×10^{-4}	2.54×10^{-4}	2.54×10^{-4}	2.54×10^{-4}	2.54×10^{-4}	4.16×10^{-4}
H_{ct}	m	1.0×10^{-6}	2.87×10^{-5}	2.87×10^{-5}	2.87×10^{-5}	2.87×10^{-5}	2.87×10^{-5}	2.87×10^{-5}	2.01×10^{-5}
H_m	m	2.3×10^{-4}	2.3×10^{-4}	2.3×10^{-4}	2.3×10^{-4}	2.3×10^{-4}	2.3×10^{-4}	1.75×10^{-4}	1.25×10^{-4}
$D_{o,ref}$	$m^2\ s^{-1}$			6.5×10^{-5}	5.22×10^{-6}			5.22×10^{-6}	5.22×10^{-6}
$D_{h,ref}$	$m^2\ s^{-1}$			3.7×10^{-5}	2.63×10^{-6}			3.76×10^{-6}	3.76×10^{-6}
K	m^2		1.76×10^{-11}	1.76×10^{-11}	1.76×10^{-11}	1.76×10^{-11}	1.76×10^{-11}	1.76×10^{-11}	1.76×10^{-11}
κ_s	$S\ m^{-1}$	120		53			53		
κ_m	$S\ m^{-1}$	17	[20]*	[20]*	[20]*	[20]*		17	[20]*
$A_s i_{a,ref}$	$A\ m^{-3}$			9.23×10^8	5.0×10^8	5.0×10^8		5.2×10^8	8.5×10^8
$A_s i_{c,ref}$	$A\ m^{-3}$		5.0×10^2	1.05×10^6	1.0×10^2	1.0×10^2		1.1×10^2	45
ε_d			0.4	0.4	0.4	0.4	0.4	0.4	0.3
α_a		1.0		0.25	1.0	1.0	0.25	1.0	1.0
α_c		0.5	0.5	0.625	0.5	0.5	0.625	0.5	0.5
$c_{h,ref}$	$mol\ m^{-3}$					56.4			
$c_{o,ref}$	$mol\ m^{-3}$	4.62				3.39			

* The value of κ_m in the model is computed by the method in [20].

ten papers all agree well with the same experimental data. This very interesting situation stimulates the authors to conduct the present study. In the following, a review will first be given on the previous parameter effects study and the model validation issue for the PEMFC.

2.3. Previous parameter effects studies and model validation discussion

Many researchers have made an investigation of the effects of parameters on the performance of fuel cells. The parameters which have been investigated include: operating parameters (i.e. temperature, humidity, pressure, flow rate, etc.), design parameters (i.e. geometrical parameters, etc.), physical parameters (i.e. porous media porosity, permeability, etc.), electrochemical parameters (i.e. specific area of catalyst layer timed by reference electrical density) and other parameters (i.e. CO poisoning, etc.).

Berning et al. [48] investigated the effects of various operating parameters such as temperature, pressure and stoichiometric flow ratio on the fuel cell performance. In addition, geometrical and material parameters such as the gas diffusion electrode thickness and porosity as well as the ratio between the channel width and the surface area were investigated. Yi and Nguyen [88] investigated the effects of the gas hydrodynamics on the performance of the air cathode of a PEM fuel cell in contact with an inter-digitated gas distributor. In addition the effects of pressure drop between the inlet and outlet channels of an inter-digitated gas distributor, the electrode height, and shoulder width on the average current density were investigated. Pasaogullari and Wang [89] developed a model to explore the two-phase flow physics in the cathode gas diffusion layer. The simulations revealed that flooding of the porous cathode reduced the rate of oxygen transport to the cathode catalyst layer. Furthermore, they indicated that the humidification level and the flow rate of reactant streams are key parameters controlling PEMFC performance and two-phase flow and transport characteristics. Jaouen et al. [16] developed a one-dimensional, steady-state agglomerate model to study the nature of mass transport limitations in the PEMFC cathode. The effect of the active layer thickness, oxygen concentration and relative humidity of the oxygen stream were investigated. Chen et al. [90] presented a two-dimensional, along-the-channel model to design fuel channels for proton exchange membrane (PEM) fuel cells. The analysis was made of the effects of some operation and design parameters, such as inlet velocity, inlet pressure, catalyst activity, height of channel, and porosity of gas-diffusion layer. Chu et al. [91] and Jeng et al. [92] made an investigation of the effects of the change of the gas diffuser layer porosity on the performance of a proton exchange membrane fuel cell. Lee et al. [93] presented a simulation of the fluid in the gas channel and the diffusion layer for the effects on the electrode variables: gas diffusion layer thickness, porosity, and distribution of pore size. Lum and McGurik [94] developed a model of the cathode of a PEMFC with an inter-digitated gas distributor with the intention of studying the effects of various operating parameters such as electrode permeability, thickness and shoulder width. Kazim et al. [95] developed a two-dimensional mathematical model to investigate the effects of parameters such as cathode porosity, inlet oxygen mole fraction, operating temperature and pressure. Hwang et al. [96] developed a three-dimensional numerical model to simulate the transport phenomena on the cathodic side of a PEMFC and compared the polarization curves of the inter-digitated flow field and parallel flow field. Recently, Li and Sabir [97] presented a review of the state-of-the-art for different bipolar plates in PEM fuel cells. Meng and Wang [98] investigated effects of electron transport through the gas diffusion layer in detail. Du et al. [99] investigated the effective proton and electronic conductivity of the catalyst layers. Chan and Tun [100] investigated the effects

of the cathode reference exchange current density multiplied by the area, reference oxygen concentration and oxygen diffusivity on the performance. Sun et al. [101] applied a two-dimensional cross-the-channel model to investigate the influence of the gas diffusion layer property and flow-field geometry such as diffusion layer diffusivity, diffusion layer conductivity, channel width-to-area ratio and diffusion layer thickness on the local reaction rate in the PEMFC cathode catalyst layer. They found that when the PEMFC uses reformate hydrogen, the PEMFC performance drops dramatically due to CO poisoning as the anode flow rate increases. Zhou and Liu [55], Chan et al. [76], Baschuk et al. [78,102], Camara et al. [103], Zhang et al. [104] and Wagner and Gülzow [105] all investigated the effects of CO poisoning on PEMFC performance. More recently, researchers started to focus on the investigation of the air-breathing PEMFC models [106–109].

In the above references the major focus mainly was concentrated on the effect of some individual parameters, the comparison of effects from different parameters and the sensitivity of the parameter variation on the final outcome of *V–I* were not their main purpose. Here the parametric sensitivity refers to what degree a parameter affects the PEMFC performance, especially the *V–I* curve. Recently, some researchers have been aware of the importance of the sensitivity issue and several papers were published. Stockie et al. [110] performed a sensitivity study. It was revealed that some geometrical and operational parameters are critical to fuel cell performance. Grujicic et al. [111] performed a sensitivity analysis to determine the effects of six parameters, including thickness of the active layer, molar diffusion volume of oxygen, molar diffusion volume of water, molar diffusion volume of nitrogen, and porosity of cathode, on the performance of PEM fuel cell based in a steady-state single-phase three-dimensional electro-chemical model. The results showed that the performance of a common PEMFC is strongly affected by these parameters. But the performance of the fuel cell specially designed by their optimizing method is essentially unaffected by these parameters. Corrêa et al. [112] presented a sensitivity analysis on the PEMFC stack. They classified the parameters according to their influence in the fuel cell stack as: insensitive, sensitive, and highly sensitive.

From Table 1 and the above-referenced papers, it can be found that the transport and electrochemical parameters involved in the numerical modeling have a wide range of variation. The present authors then examined how the values of parameters are obtained in the numerical simulation papers. It was found that there are three methods to get the values of the PEMFC parameters. One method is the direct measurement, i.e., parameters are measured via experiments. For example, Lee et al. [113] prepared a precise impedance measurement system based on two-probe and four-probe methods to measure the impedance and consequent proton conductivity of the Nafion membrane. Saito et al. [114] measured the ionic conductivity, water transference coefficient, water permeability and diffusion coefficients of the water and the Li^+ cation for several membranes. Parthasarathy et al. [115] and Zhang et al. [116] measured the kinetic and mass transport properties for the oxygen reduction reaction in the membrane. However, some parameters are very difficult to measure, or even cannot be determined by experimental methods and must be estimated [9]. Therefore the second method to obtain the parameters is via an appropriate computational or fitting method. Suares and Hoo [117] estimated four parameters such as the exchange current density for oxygen reaction, diffusion coefficient of water, evaporation and condensation rate and overall heat-transfer coefficient using voltage–current data. Carnes and Djilali [80] defined an algorithm for nonlinear least squares fitting to estimate the effective membrane conductivity, exchange current densities and oxygen diffusion coefficients in a one-dimensional PEMFC model. Berg et al. [118] estimated four parameters such as exchange current, membrane water transfer coefficient, effective oxygen diffusivity and average membrane resistance using a one-dimensional PEMFC model based on [34]. Thamapan et al. [119] performed a parameters estimation for the membrane conductivity submodels using curve fitting. Guo et al. [120] fitted cathode catalyst layer parameters such as porosities, reference current densities and effective diffusion coefficients using a one-dimensional cathode catalyst layer model. However, for most of the simulation researchers, the parameters were obtained from models given by other research groups, which constituted the third method to obtain the parameters. Thus it can be seen that one of the major reason that some transport and electrochemical parameter variation ranges are quite large is simply because of the inherent difficulty and complexity in experimental measurement. Actually because of the small size of the gas channels and the small thickness of the diffusion layers, catalyst layers and membrane, it is very difficult to measure the flow and species distributions in these regions. This situation should be taken into account when the fuel cell model validation issue is concerned.

From previous studies, the transport and electrochemical parameters can be classified according to their influence on the model results as insensitive and sensitive. The permeability and solid phase conductivity consist of the insensitive parameters. Most of the other parameters such as diffusion layer porosity, membrane phase conductivity, cathode reference exchange density multiplied by area, oxygen diffusivity, reference oxygen concentration et al. are the sensitive parameters.

As far as the validation criterion is concerned only very recently researchers in the international community have shown their concern on whether the polarization curve only is enough for the model validation (the CFD/NHT model validation). Hakenjos et al. [121] pointed out that for the validation of multidimensional models, using only the polarization curve is not sufficient, and they performed an additional comparison between the measured and simulated electrical current distributions. Lum and McGuirk [33] also used a two-step validation approach: global validation by the polarization curve and local validation by the distribution of local current density obtained from a segmented fuel cell. In [122] an interesting example was presented: a three-dimensional PEMFC model was used for a single channel fuel cell. In one case the ionic resistance in two catalyst layers was included, while in the other case these resistances were neglected. By adjusting the kinetics, the numerical simu-

lation results for the current density of the two cases were exactly the same at a voltage of 0.75 V. Thus the authors proposed that apart from the global validation, the local distribution of current density should be added in order to validate a comprehensive PEMFC model.

It can be seen that after about 20 years, in numerical modeling of PEMFC performance researchers have become aware that the polarization curve comparison is enough for the validation of a comprehensive model. This work tries first to perform a comprehensive study of the parameter sensitivity for an advanced PEMFC model based on some numerical results to give a detailed discussion of how to validate a simulation model. We finally found that even the proposed two-step validation approach is not enough to validate a model, hence a third validation index, which is relatively easy to be measured is proposed. The sensitivity examination results and the discussion of the model validation issue will be presented in the companion paper [123].

3. Present model description

The computational domain of the present model is shown in Fig. 1. The conventional parallel flow fields are adopted in this model. The model assumes that the fuel cell structure is repeated periodically along the *y*-direction. Neglecting the end effects for each gas channel, it can be regarded that the process in each channel is identical. Hence, to save computation time, half of a gas channel can be taken as the computational domain as shown in Fig. 2. Dry air is fed into the cathode channel, whereas humidified hydrogen is supplied to the anode channel.

The assumptions adopted in the present model are:

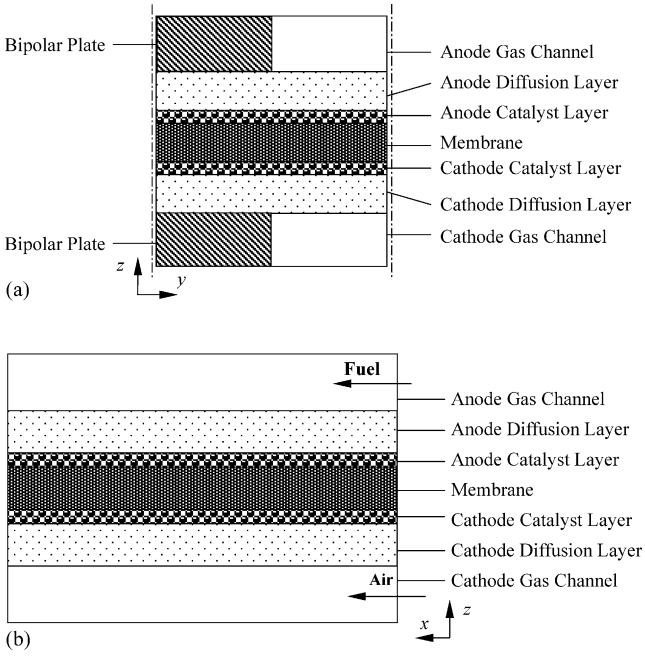

Fig. 2. The two-dimensional cross-sections of the computational domain: (a) *y*–*z* cross-section; (b) *x*–*z* cross-section.

(1) The fuel cell operates under a steady-state condition.
(2) The gas mixture is an incompressible ideal fluid.
(3) The flow in the gas channels is laminar.
(4) The diffusion layer, catalyst layer and membrane are isotropic and homogeneous, and the membrane is considered impervious for reactant gases.
(5) Ohmic heating in the bipolar plates and the diffusion layers are neglected due to their high conductivities.
(6) Ohmic potential drops in the diffusion layers and bipolar plates are neglected due to their high electrical conductivities.
(7) The contact resistance between any two parts in the fuel cell is neglected.

3.1. Model equations

The three-dimensional, two-phase, non-isothermal model consists of non-linear, coupled partial differential equations representing the conservation of mass, momentum, species, charge and energy. The conservation equations are described in the vector form as follows.

Mass conservation equation:

$$\nabla \cdot (\rho_g \mathbf{u}_g) = S_m \tag{1}$$

Momentum conservation equation:

$$\frac{1}{\varepsilon(1-s)}\nabla \cdot (\rho_g \mathbf{u}_g \mathbf{u}_g) = -\nabla p_g + \frac{1}{\varepsilon(1-s)}\nabla \cdot (\mu_g \nabla \mathbf{u}_g) + S_u \tag{2}$$

Species conservation equation:

$$\nabla \cdot (\rho_g \mathbf{u}_g X_k) = \nabla \cdot (\rho_g D_{k,\mathrm{eff}} \nabla X_k) + S_k \tag{3}$$

where the index refers to different species, including oxygen, hydrogen and water vapor.

Electrical charge equations:

$$\nabla \cdot (\kappa_s \nabla \phi_s) + S_{\phi,s} = 0 \tag{4}$$

$$\nabla \cdot (\kappa_m \nabla \phi_m) + S_{\phi,m} = 0 \tag{5}$$

Energy conservation equation:

$$\nabla \cdot (\rho_g \mathbf{u}_g T) = \nabla \cdot (\lambda_{\mathrm{eff}} \nabla T) + S_T \tag{6}$$

Source terms in the above governing equations (S_m, S_u, S_k, $S_{\phi,s}$, $S_{\phi,m}$, and S_T) are summarized in Table 2 for various sub-regions of the fuel cell. The source term in momentum conservation equation, S_u, represents Darcy's drag force imposed by the pore walls on the fluid within the pores, which usually results in a significant pressure drop across the porous medium. Eq. (2) is the general expression of the momentum equation. In the gas channel region, the porosity ε becomes unity and the coefficient of permeability approaches infinity, hence Eq. (2) resumes a conventional form of the momentum equation. In the porous medium region, the general momentum conservation equation

Table 2
Source terms for governing equations in various regions of a PEMFC

	Gas channel	Diffusion layer	Catalyst layer	Membrane
Mass	$S_m = 0$	$S_m = 0$	Anode: $S_m = S_h + S_w$, cathode: $S_m = S_o + S_w$	$S_m = 0$
Momentum	$S_u = 0$	$S_u = -\frac{\mu_g}{KK_{rg}}\mathbf{u}_g$	$S_u = -\frac{\mu_g}{KK_{rg}}\mathbf{u}_g$	$S_u = 0$
Species O_2	$S_o = 0$	$S_o = 0$	$S_o = -(i_c/4F)M_o$	$S_o = 0$
H_2	$S_h = 0$	$S_h = 0$	$S_h = -(i_a/2F)M_h$	$S_h = 0$
Charge				
Solid phase	$S_{\phi,s} = 0$	$S_{\phi,s} = 0$	$S_{\phi,s} = -I$	$S_{\phi,s} = 0$
Membrane phase	$S_{\phi,m} = 0$	$S_{\phi,m} = 0$	$S_{\phi,m} = I$	$S_{\phi,m} = 0$
Energy	$S_T = 0$	$S_T = 0$	$S_T = i\left(\eta + T\frac{dV_{oc}}{dT}\right) + \frac{I^2}{\kappa_m}$	$S_T = \frac{I^2}{\kappa_m}$

reduces to the expression of Darcy's law:

$$\mathbf{u}_g = -\frac{K \cdot K_{rg}}{\mu_g}\nabla p_g \tag{7}$$

$$\boldsymbol{u}_l = -\frac{K \cdot K_{rl}}{\mu_l}\nabla p_l \tag{8}$$

The source term in mass conservation (S_m) and species conservation equations for O_2 and H_2 (S_k) are the volumetric sink or source terms due to the electrochemical reactions in the catalyst layer, and they are zero in other parts of the computational domain. The source term in the energy conservation equation (S_T) represents the sum of the reversible heat release and irreversible heat generation [56].

In Eqs. (1)–(8) and in Table 2 a lot of parameters and variables need to be further determined. They are described as follows.

The liquid water saturation that appears in Eq. (2) is defined as the volume fraction of liquid water in the porous media, that is

$$s = \frac{V_l}{1 - V_S} \tag{9}$$

In order to derive the governing equation for the liquid water saturation the mass conservation equation of liquid water is needed:

$$\nabla \cdot (\rho \mathbf{u}_l) = -S_w \tag{10}$$

The so-called capillary pressure p_c is defined as the difference of the pressure between the gas and the liquid:

$$p_c = p_g - p_l \tag{11a}$$

This pressure is assumed to be a function of liquid water saturation [62,124]:

$$p_c = \sigma\left(\frac{\varepsilon}{K}\right)^{1/2}[1.417(1-s) - 2.120(1-s)^2 + 1.263(1-s)^3] \tag{11b}$$

With Eqs. (1), (7), (8), (10), (11a) and (11b), the liquid water saturation equation can be derived, which says:

$$\nabla \cdot \left(\rho_l \frac{\eta_g}{\eta_l}\frac{K_{rl}}{K_{rg}}\mathbf{u}_g\right) = \nabla \cdot (\rho_l D_c \nabla s) - S_w \tag{12}$$

The source term for the water vapor equation (included in Eq. (3) when the index k takes the corresponding value) is the same for the liquid water saturation equation, Eq. (12), and it represents the interfacial mass-transfer rate of water between the gas and liquid phases. It is substantially similar to the form in [39]:

$$S_w = h_m \varepsilon s(\rho_g X_{wsat} - \rho_g X_w) \tag{13}$$

where h_m is the evaporation and condensation rate and X_{wsat} is the mass fraction of water vapor when the mixture is saturated and is related to the saturation pressure p^{sat} at operating temperature, which is given by [36]:

$$\log_{10} p^{sat} = -2.1794 + 0.02593T - 9.1837 \times 10^{-5}T^2 + 1.4454 \times 10^{-7}T^3 \tag{14}$$

The determinations of a number of diffusivities are now described. The diffusivity in Eq. (3) can be determined as follows. The value of the species in the gas channel is a function of temperature and pressure, and is determined by following equation [56]:

$$D_{k,eff} = D_{k,ref}(T/T_{ref})^{3/2}(p_{ref}/p) \tag{15}$$

where $D_{k,ref}$ is the reference value at T_{ref} and p_{ref}. In the porous media region the diffusivity of the species can be described by the Bruggeman model [56]:

$$D_{k,eff} = \varepsilon^{1.5} D_{k,ref} \tag{16}$$

The capillary diffusion coefficient D_c in Eq. (12) is given by [82]:

$$D_c = -\frac{s^3 \lambda_g K}{\eta_l}\frac{dp_c}{ds} \tag{17}$$

$$\lambda_g = \frac{\frac{K_{rg}}{\nu_g}}{\frac{K_{rl}}{\nu_l} + \frac{K_{rg}}{\nu_g}} \tag{18}$$

where ν and σ are kinetic viscosity and surface tension, respectively. The relative permeabilities for the liquid and gas phases are represented by [40]:

$$K_{rl} = s^3, \qquad K_{rg} = (1-s)^3 \tag{19}$$

Now attention is turned to the electrical charge equations. The source terms in Eqs. (4) and (5) are directly related to the electrochemical reaction expressed by the electrical current, which

is given by Bulter–Volumer equation:

$$\text{Anode}: \quad i = A_s i_{a,ref}\left(\frac{c_h}{c_{h,ref}}\right)^{1/2} \times\left\{\exp\left[\frac{\alpha_a n_a F}{RT}\eta_a\right]-\exp\left[-\frac{(1-\alpha_a)n_a F}{RT}\eta_a\right]\right\} \tag{20}$$

$$\text{Cathode}: \quad i = A_s i_{c,ref}\frac{c_o}{c_{o,ref}} \times\left\{\exp\left[\frac{\alpha_c n_c F}{RT}\eta_c\right]-\exp\left[-\frac{(1-\alpha_c)n_c F}{RT}\eta_c\right]\right\} \tag{21}$$

The proton conductivity k_m in Eq. (5) is related with the water content of the membrane, λ, which is in turn a function of the water activity, a [20]:

$$\kappa_m = (0.5139\lambda - 0.326)\exp\left[1268\left(\frac{1}{303}-\frac{1}{T}\right)\right] \tag{22}$$

$$\lambda = \begin{cases} 0.043 + 17.81a - 39.85a^2 + 36.0a^3 & 0 < a \le 1 \\ 14 + 1.4(a-1) & 1 < a \le 3 \end{cases} \tag{23}$$

$$a = \frac{\omega_w RT}{P^{sat}} \tag{24}$$

where ω_w is the molar fraction of water vapor.

Once the membrane phase potential, ϕ_m and the proton conductivity on the membrane, k_m are obtained, local current density, I, can be calculated by

$$I = -\kappa_m \nabla\phi_m \tag{25}$$

The overpotential is described as

$$\eta = \eta_{tot} - |\phi_s - \phi_{s,ref}| - |\phi_m - \phi_{m,ref}| \tag{26}$$

where η_{tot} is the total overpotential of anode or cathode, $\phi_{s,ref}$ the solid phase potential at reference state and $\phi_{m,ref}$ is the membrane phase potential at reference state. For the solid phase potential, the potential at the interface between the anode current collector and the diffusion layer is zero, and for the membrane phase potential, the potential at the interface between the anode catalyst layer and the membrane is set to be zero also.

The operating potential of the cell is then calculated by

$$V_{cell} = V_{oc} - \eta_{a,tot} - \eta_{c,tot} - \eta_{m,pro} \tag{27}$$

where $\eta_{m,pro}$ is the Ohmic overpotential in the membrane, and V_{oc} is the open circuit potential, which is calculated by [21]:

$$V_{oc} = 1.23 - 0.9\times10^{-3}(T-298) + 2.3\frac{RT}{4F}\log(p_h^2 p_o) \tag{28}$$

Table 3
Grid-independence test

Grid size	I_{av} (A cm^{-2})
12 × 12 × 40	0.8034
22 × 12 × 40	0.8045
32 × 12 × 40	0.8058
32 × 22 × 40	0.8072
42 × 22 × 40	0.8074
32 × 32 × 40	0.8080

It should be noted that although the model equations of the present model are mainly copied from existing papers, the present two-phase model is different from all of the existing models. The previous papers known to the authors presented either an isothermal one-dimensional model [20], or isothermal two-dimensional models [36,39,40,62,124], or a single-phase three-dimensional model [56] or an isothermal two-phase three-

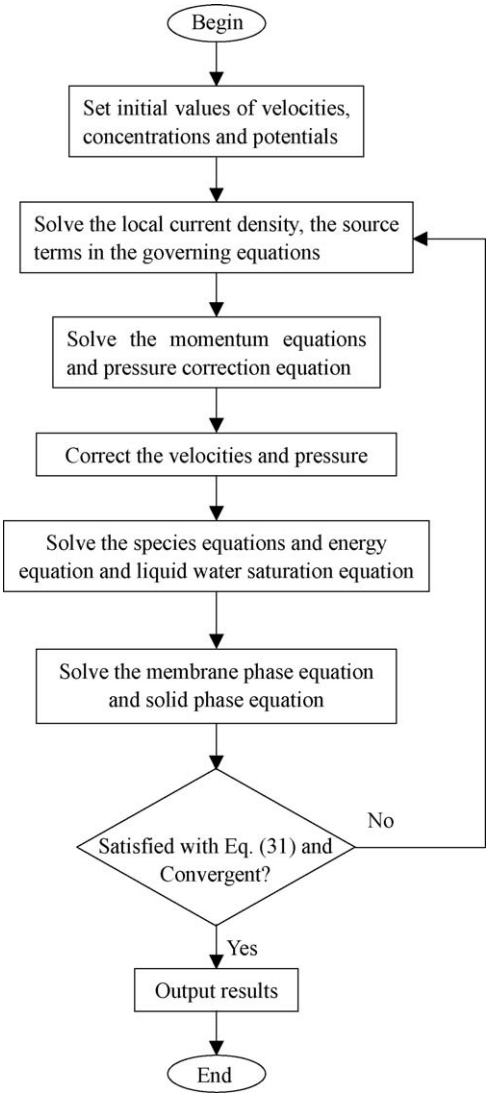

Fig. 3. Flow diagram of the solution procedure.

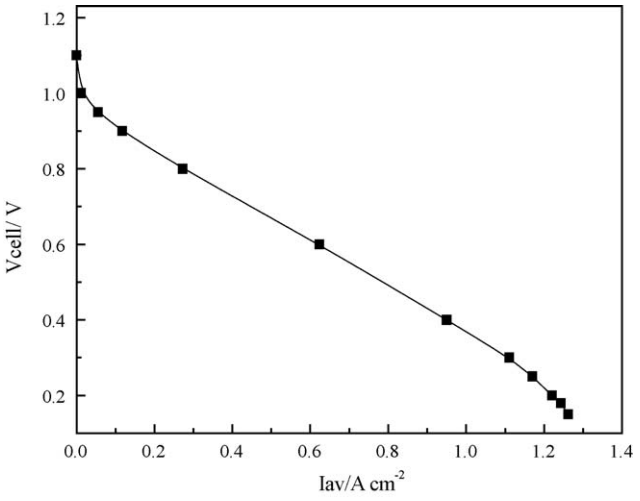

Fig. 4. Polarization curve of PEMFC on the base case: (a) $V_{cell} = 0.8$; (b) $V_{cell} = 0.3$.

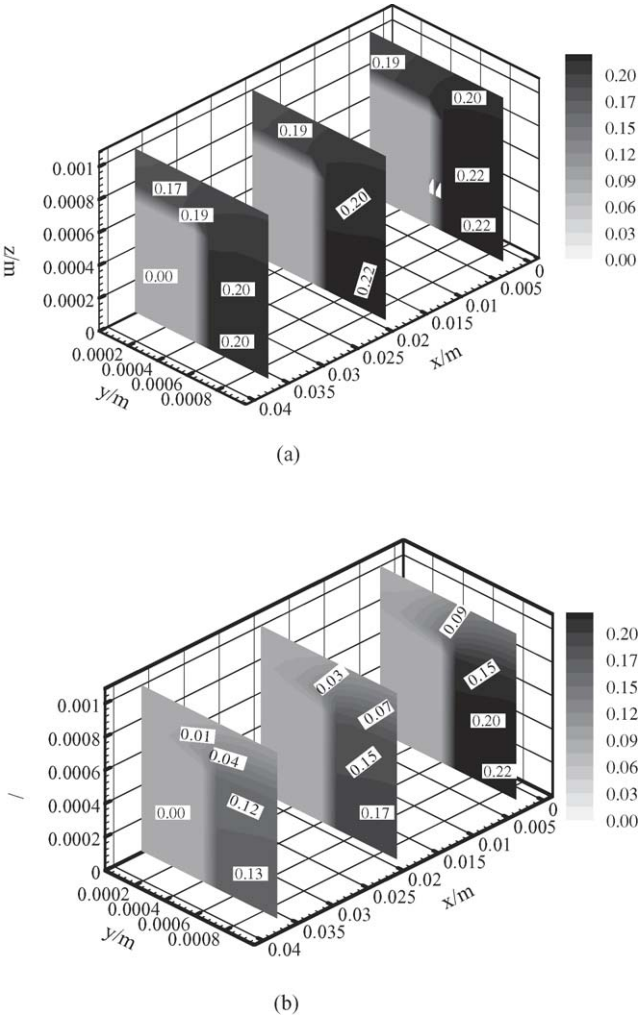

Fig. 5. Oxygen mass fraction distribution in the cathode: (a) $V_{cell} = 0.8$; (b) $V_{cell} = 0.3$.

dimensional model [82]. However, the present model is a three-dimensional, two-phase, non-isothermal model. Furthermore, the present model presents a method in detail to obtain the voltage versus current curve of PEMFC. This method will be described in Section 3.3.

3.2. Boundary conditions

In the x–z plane, symmetrical conditions are adopted. That is, the gradient in the y-direction of each variable is zero.

At the gas channel inlet, the temperature and gas species concentrations are assumed to be uniform. The inlet velocities are specified by

$$u_{a,in} = \zeta_a \frac{I_{ref}}{2F} A_m \frac{RT_{a,in}}{p_{a,in}} \frac{1}{X_{o,in}} \frac{1}{A_{ch}} \tag{29}$$

$$u_{c,in} = \zeta_c \frac{I_{ref}}{4F} A_m \frac{RT_{c,in}}{p_{c,in}} \frac{1}{X_{h,in}} \frac{1}{A_{ch}} \tag{30}$$

where ζ_a and ζ_c are the reactant stoichiometric flow ratio of anode and cathode, respectively, they are defined as the ratio of the amount of reactant supplied to the amount of reaction to generate the specified reference current density I_{ref}. A_m is the geometrical area of the membrane and A_{ch} is the cross-sectional area of the gas channel.

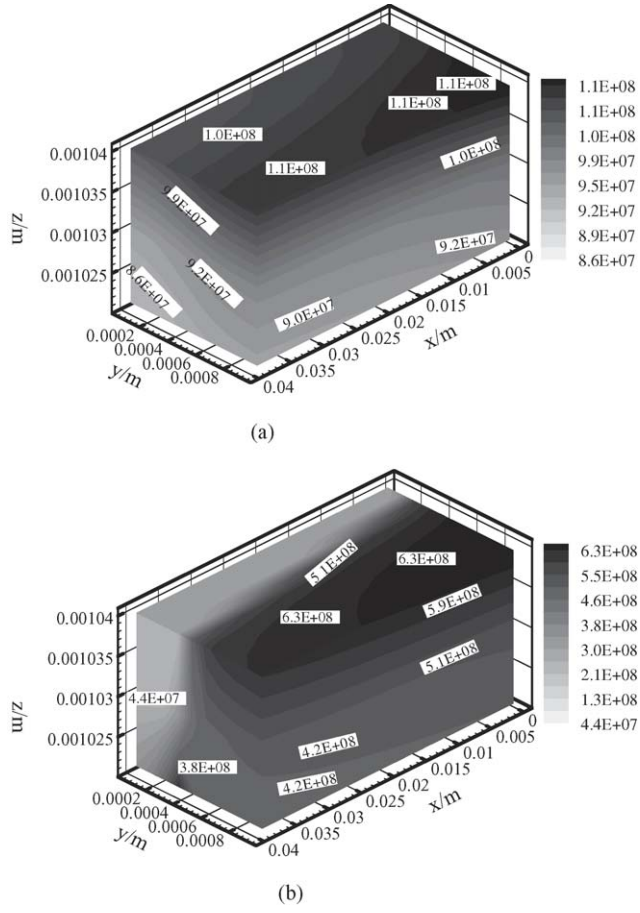

Fig. 6. Local current density distribution in the cathode catalyst layer: (a) $V_{cell} = 0.8$; (b) $V_{cell} = 0.3$.

A local one-way assumption is adopted to give the gas channel outlet velocity condition, and is then corrected by a global mass conservation constraint [125].

At the body surface, the no-slip condition is applied for the velocity and non-permeable condition of the species mass fraction.

For the liquid water saturation, the computational domain involves two diffusion layers, two catalyst layers and a membrane. At the interface between the gas channel and the diffusion layer, the liquid water velocity is set to zero.

The computational domain for the electrical charge equations involves the anode catalyst layer, the membrane and the cathode catalyst layer. The boundary conditions are described as follows:

at the surface of the anode catalyst layer : $\phi_s = 0$,

$$\frac{\partial \phi_m}{\partial z} = 0$$

at the surface of the cathode catalyst layer : $\phi_s = V_{cell}$,

$$\frac{\partial \phi_m}{\partial z} = 0$$

3.3. Numerical procedures

The governing equations, together with the boundary conditions are discretized by the finite volume method. The SIMPLEC algorithm [125] is utilized to deal with the coupling of the velocity and the pressure. Since all governing equations are coupled with each other, they ought to be solved simultaneously with an iterative method. The solution is considered to be convergent when the relative error of each dependent variable between two consecutive iterations is less than 1.0×10^{-5}.

The grid system used is $32 \times 22 \times 40$. To simulate the local transport phenomena in the fuel cell, the grid arrangement at z-direction is non-uniform. The grid-independence test is performed on six grid systems. The results of the average current density computed by the model under different grid systems when the fuel cell operating voltage is 0.5 V are summarized in Table 3. Considering both accuracy and economics, the grid system of $32 \times 22 \times 40$ was selected for present research.

There are generally two ways of obtaining the voltage versus current curve: either the operating current density is given and different potential losses are calculated, or the so-called

Table 4
Model parameters for basic case

Parameter	Symbol	Value	Reference
Gas channel length	L	0.04 m	
Gas channel width	W	7.62×10^{-4} m	
Gas channel height	H_{ch}	7.62×10^{-4} m	
Diffusion layer height	H_d	2.54×10^{-4} m	
Catalyst layer height	H_{ct}	2.87×10^{-5} m	
Membrane height	H_m	2.3×10^{-4} m	
Land area width	W_{cc}	7.62×10^{-4} m	
Faraday's constant	F	96487 C mol^{-1}	
Gas channel inlet temperature	T_{in}	353 K	
Anode/cathode pressure	p_a/p_c	1/1 atm	
Electron number of anode reaction	n_a	4	
Electron number of cathode reaction	n_c	2	
Fuel/air stoichiometric flow ratio	ζ_a/ζ_c	3/3	[48]
Relative humidity of inlet fuel	RH_a	100%	[56]
Relative humidity of inlet air	RH_c	0	[56]
Oxygen mass fraction of inlet air	X_o	0.23	
H_2 diffusion coefficient at reference state	$D_{h,ref}$	0.915×10^{-4} m^2 s^{-1}	[48]
O_2 diffusion coefficient at reference state	$D_{o,ref}$	0.22×10^{-4} m^2 s^{-1}	[48]
Water vapor diffusion coefficient at reference state	$D_{w,ref}$	0.256×10^{-4} m^2 s^{-1}	[48]
Anode exchange current density multiply specific area	$A_s i_{a,ref}$	5.0×10^7 A m^{-3}	
Cathode exchange current density multiply specific area	$A_s i_{c,ref}$	120 A m^{-3}	
Hydrogen reference concentration	$c_{h,ref}$	56.4 mol m^{-3}	[21]
Oxygen reference concentration	$c_{o,ref}$	3.39 mol m^{-3}	[21]
Anode transfer coefficient	α_a	0.5	[56]
Cathode transfer coefficient	α_c	0.5	[56]
Porosity of diffusion layer	ε_d	0.3	[68]
Porosity of catalyst layer	ε_{ct}	0.28	[81]
Absolute permeability	K	1.76×10^{-11} m^2	[36]
Solid phase conductivity	κ_s	53 S m^{-1}	[7]
Membrane phase conductivity	κ_m	6 S m^{-1}	[48]
Surface tension	σ	0.0625 N m^{-1}	[40]
Evaporation and condensation rate	h_m	100 s^{-1}	[80]
Current collector thermal conductivity	k_c	150 W m^{-1} K^{-1}	[36]
Diffusion layer thermal conductivity	k_d	150 W m^{-1} K^{-1}	[36]
Membrane thermal conductivity	k_m	0.95 W m^{-1} K^{-1}	[56]

potentiostatic approach is used, where the cell potential is set and the current density is calculated [36]. We chose the second approach for the simulation. By giving the initial values of the anode total overpotential and cathode total overpotential, the current density can be obtained, and the Ohmic losses can be calculated. Then the anode total overpotential and cathode total overpotential are corrected by the constraint that the anode current should be equal to cathode current, that is

$$I_{\mathrm{av}} = \frac{1}{A_{\mathrm{m}}} \sum (i_{\mathrm{a}} V_{\mathrm{CV}}) = \frac{1}{A_{\mathrm{m}}} \sum (i_{\mathrm{c}} V_{\mathrm{CV}}) \tag{31}$$

where I_{av} and V_{CV} are the cell average current density and the volume of the control volume, respectively. Such an iterative solution procedure is shown in Fig. 3.

To conduct the modeling simulation, a great number of parameters are required. The parameters of the basic case and the corresponding references are all listed in Table 4. The numerical results of the basic case are regarded as the references for further parameter sensitivity examination.

4. Results and discussion for the basic case

In this section, the PEMFC polarization curve for the basic case will be first presented. Then the distribution of the oxygen mass fraction in the cathode, local current density, liquid water saturation and temperature will be presented in order.

The polarization curve of the basic case is shown in Fig. 4. It follows the general variation trend observed for the PEMFC in many references and will not be further discussed.

Fig. 5 shows profiles for the oxygen mass fraction in the cathode, including the gas channel and diffusion layer. At high cell voltages, the oxygen mass fraction is relatively uniform. Whereas at low cell voltages, the oxygen mass fraction is far from being uniform, which implies that the local current density is non-uniformly distributed in the catalyst layer at a low cell voltage since the local current density is dependent on the oxygen concentration.

Fig. 6 shows the distribution of local current density in the cathodic catalyst layer. It can be seen that the distribution is quite uniform at high cell voltages. The local current density is somewhat lower over the shoulder than over the channel. The

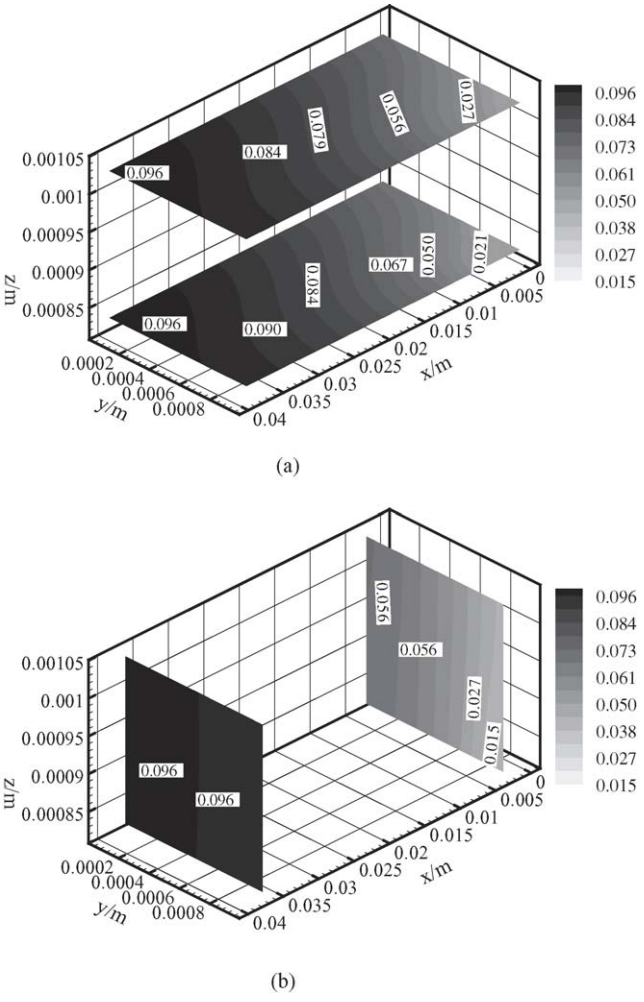

Fig. 7. Liquid water saturation distribution in the cathode electrode ($V_{\mathrm{cell}} = 0.6$): (a) x–y plane; (b) y–z plane.

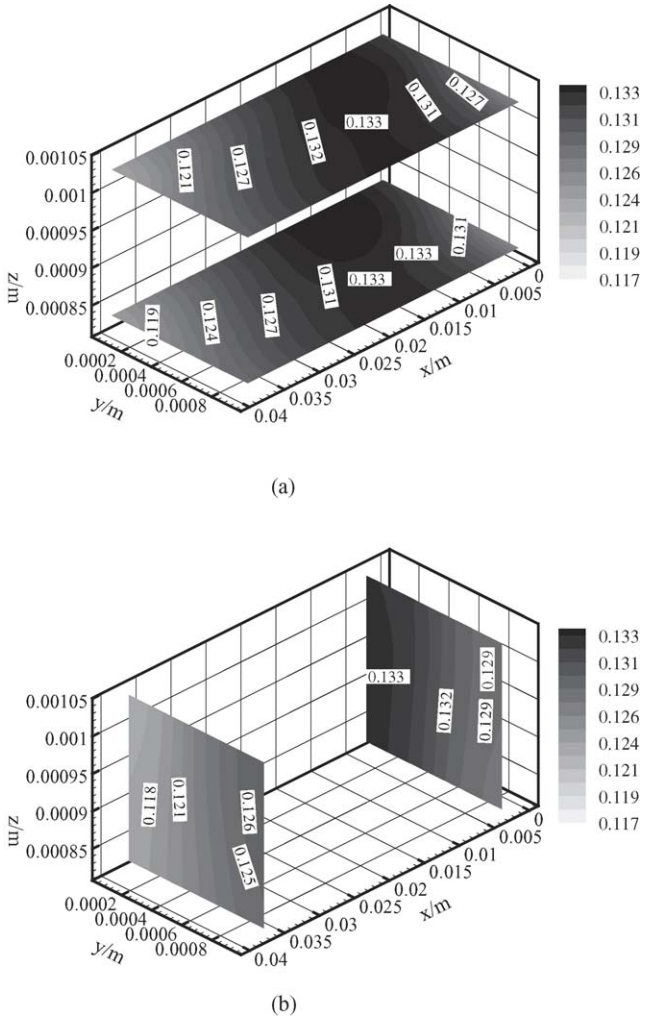

Fig. 8. Liquid water saturation distribution in the cathode electrode ($V_{\mathrm{cell}} = 0.3$): (a) x–y plane; (b) y–z plane.

minimum current density is located at the corner of the catalyst layer over the shoulder adjacent to the diffusion layer. While at low cell voltages, the distribution pattern becomes very different from that at high cell voltages. The minimum current density is located at the corner of the catalyst layer over the shoulder adjacent to membrane, and the current density distribution is very non-uniform. The phenomena result from the mass transfer

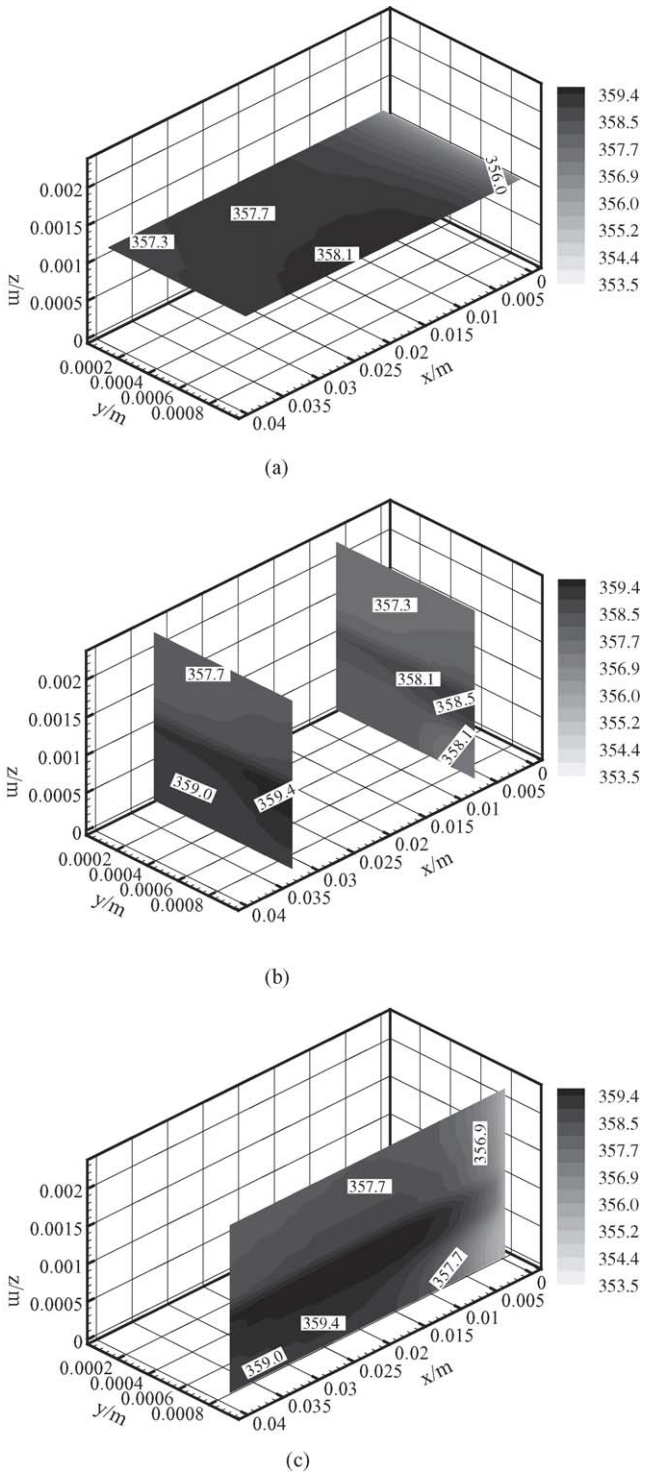

Fig. 9. Temperature distribution in the PEMFC ($V_{cell} = 0.6$): (a) x–y plane; (b) y–z plane; (c) x–z plane.

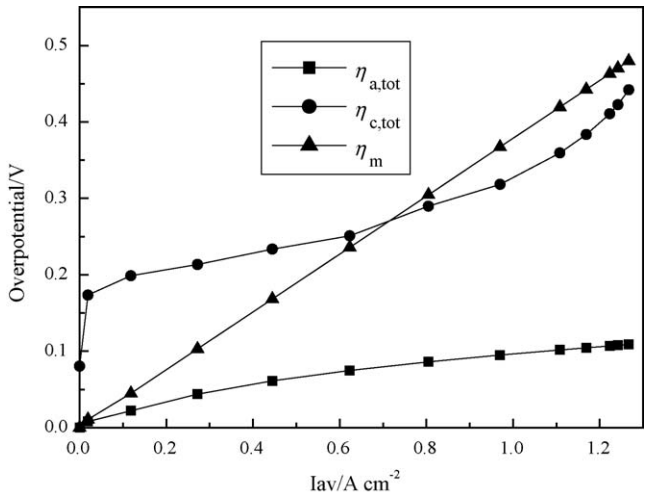

Fig. 10. Cathodic and anodic overpotentilas vs. cell voltage.

limitation of oxygen. The oxygen concentration decreases along the z-direction close to the membrane due to consumption and mass transport resistance.

Now the liquid water saturation in the cathode diffusion layer and catalyst layer is discussed. The results are shown in Figs. 7 and 8. Fig. 7 shows that at high cell voltages, the liquid water saturation is lower and relatively uniform, and it increases gradually along the direction from the gas channel inlet to the outlet. The maximum liquid saturation is located at the corner of the catalyst layer over the shoulder adjacent to the membrane. Fig. 8 shows that at low cell voltages, the liquid water saturation distribution is very different from that at high cell voltages. The liquid water saturation in the domain vary significantly, and the maximum value is not at the corner of the catalyst layer over the shoulder adjacent to membrane but at the corner of catalyst near the gas channel inlet. The reason is that at that point, the oxygen mass fraction reaches a maximum value and the generated liquid water cannot be extracted in time.

Fig. 9 shows the temperature distribution in the PEMFC when the cell voltage is 0.6 V. The results show that the temperature at the cathode side is higher that at the anode side. The maximum temperature located at the cathode catalyst layer over the gas channel is due to reversible and irreversible entropy production. The maximum temperature increase is about 6 °C. Berning et al. [48] simulated the maximum temperature increase as about 3 °C when the average current density is 1.2 A cm^{-2}. Whereas the result modeled by Ju et al. [56] was over 10 °C at $V_{cell} = 0.6$. This paper gives an intermediate result.

The variations of the cathodic and anodic overpotentials with the current density are presented in Fig. 10. It is interesting to note that in most of the previous studies, such information was usually not provided. To the authors' knowledge, only Ref. [38] presented such information. Our results show [123] that such information is useful for the validation of a model.

5. Conclusions

A comprehensive review of PEMFC models in the open literature was conducted. From this review it was found that at

least 10 different models cited the same test data for the *V–I* curve to verify their correctness, while the physical and/or electrochemical parameters involved in different models were quite different, not only different in quantity but also different in the order of magnitude. This situation stimulated the present authors to perform a sensitivity study for the major parameters and to examine whether the *V–I* curve only can be serve as the model verification index.

A three-dimensional, two-phase and non-isothermal model was developed based on the existing models. The simulated results include the polarization curve, the oxygen mass fraction distribution in the cathode, the local current density distribution in the cathode catalyst layer, the liquid water saturation distribution in the cathode electrode, the cathodic and anodic overpotentials versus current density, and the temperature distribution in the PEMFC. Generally speaking, these simulated results qualitatively agree with the existing results in the literature.

The parameter sensitivity examination results and discussion of model validation are reported in the companion paper.

Acknowledgement

This work is supported by the National Natural Science Foundation of China (No. 50236010, 50425620).

References

[1] S. Gamburzev, A.J. Appleby, Recent progress in performance improvement of the proton exchange membrane fuel cell (PEMFC), J. Power Sources 107 (2002) 5–12.
[2] D. Hyun, J. Kim, Study of external humidification method in proton exchange membrane fuel cell, J. Power Sources 126 (2004) 98–103.
[3] S.Y. Ahn, Y.C. Lee, H.Y. Ha, S.A. Hong, I.H. Oh, Effect of the ionomers in the electrode on the performance of PEMFC under non-humidifying conditions, Electrochim. Acta 50 (2004) 673–676.
[4] M. Grujicic, K.M. Chittajallu, Design and optimization of polymer electrolyte membrane (PEM) fuel cells, Appl. Surf. Sci. 227 (2004) 56–72.
[5] A.R. Mather, A.B. Sadiq, A.K. Haroun, A.J. Shahad, Optimization study of proton exchange membrane fuel cell performance, Turk. J. Eng. Environ. Sci. 29 (2005) 235–240.
[6] K.Z. Yao, K. Karan, K.B. McAuley, P. Oosthuizen, B. Peppley, T. Xie, A review of mathematical models for hydrogen and direct methanol polymer electrolyte membrane fuel cells, Fuel Cells 4 (1/2) (2004) 3–29.
[7] E.A. Ticianelli, C.R. Derouin, S. Srinivasan, Localization of platinum in low catalyst loading electrodes to attain high power densities in SPE fuel cells, J. Electroanal. Chem. 251 (1988) 275–295.
[8] E.A. Ticianelli, C.R. Derouin, A. Redondo, S. Srinivasan, Methods to advance technology of proton exchange membrane fuel cells, J. Electrochm. Soc. 135 (9) (1988) 2209–2214.
[9] N.P. Siegel, M.W. Ellis, D.J. Nelson, M.R. von Spakovsky, A two-dimensional computational model of a PEMFC with liquid water transport, J. Power Sources 128 (2004) 173–184.
[10] D. Natarajan, T.V. Nguyen, Three-dimensional effects of liquid water flooding in the cathode of a PEM fuel cell, J. Power Sources 115 (2003) 66–80.
[11] A.A. Kulikovsky, J. Divisek, A.A. Kornyshev, Modeling the cathode compartment of polymer electrolyte fuel cells: dead and active reaction zones, J. Electrochem. Soc. 146 (11) (1999) 3981–3991.
[12] C. Marr, X. Li, Composition and performance modeling of catalyst layer in a proton exchange membrane fuel cell, J. Power Sources 77 (1999) 17–27.
[13] K. Broka, P. Ekdunge, Modeling the PEM fuel cell cathode, J. Appl. Electrochem. 27 (1997) 281–289.
[14] K.T. Jeng, C.P. Kuo, S.F. Lee, Modeling the catalyst layer of a PEM fuel cell cathode using a dimensionless approach, J. Power Sources 128 (2004) 145–151.
[15] D. Bevers, M. Wöhr, Simulation of a polymer electrolyte fuel cell electrode, J. Appl. Electrochem. 27 (1997) 1254–1264.
[16] F. Jaouen, G. Lindbergh, G. Sundholm, Investigation of mass-transport limitations in the solid polymer fuel cell cathode, J. Electrochem. Soc. 149 (4) (2002) A437–A447.
[17] K. Scott, P. Argyropoulos, A current distribution model of a porous fuel cell electrode, J. Electroanal. Chem. 567 (2004) 103–109.
[18] Y.P. Sun, K. Scott, The influence of mass transfer on a porous fuel cell electrode, Fuel Cells 4 (1/2) (2004) 30–38.
[19] K.V. Zhukovsky, Three dimensional model of oxygen transport in a porous diffuser of a PEM fuel cell, AIChE J. 49 (12) (2003) 3029–3036.
[20] T.E. Springer, T.A. Zawodzinski, S. Gottesfeld, Polymer electrolyte fuel cell model, J. Electrochem. Soc. 138 (8) (1991) 2334–2342.
[21] D.M. Bernardi, M.W. Verbrugge, A mathematical model of the solid-polymer-electrolyte fuel cell, J. Electrochem. Soc. 139 (9) (1992) 2477–2491.
[22] T. Okada, G. Xie, O. Gorseth, S. Kjelstrup, N. Nakamura, T. Arimura, Ion and water transport characteristics of Nafion membranes as electrolytes, Electrochim. Acta 43 (24) (1998) 3741–3747.
[23] P. Futerko, I.M. Hsing, Two-dimensional finite-element method study of the resistance of membranes in polymer electrolyte fuel cells, Electrochim. Acta 45 (2000) 1741–1751.
[24] H. Zhu, R.J. Kee, A general mathematical model for analyzing the performance of fuel-cell membrane-electrode assemblies, J. Power Sources 117 (2003) 61–74.
[25] K.A. Mauritz, R.B. Moore, State of understanding of Nafion, Chem. Rev. 104 (2004) 4535–4585.
[26] D.M. Bernardi, Water-balance calculations for solid polymer-electrolyte fuel cell, J. Electrochem. Soc. 137 (8) (1990) 3344–3350.
[27] D.M. Bernardi, M.W. Verbrugge, Mathematical model of gas diffusion electrode bounded to a polymer electrolyte, AIChE J. 37 (8) (1991) 1151–1163.
[28] T.E. Springer, M.S. Wilson, S. Gottesfeld, Modeling and experimental diagnostics in polymer electrolyte fuel cell, J. Electrochem. Soc. 140 (12) (1993) 3513–3526.
[29] M. Eikerling, Y.I. Kharkats, A.A. Kornyshev, Y.M. Volfkovicnh, Phenomenological theory of electro-osmotic effect and water management in polymer electrolyte protoncondcuting membrane, J. Electrochem. Soc. 145 (8) (1998) 2684–2699.
[30] J.J. Baschuk, X. Li, Modeling of polymer electrolyte membrane fuel cells with variable degree of water flooding, J. Power Sources 86 (2000) 181–196.
[31] A. Rowe, X. Li, Mathematical modeling of proton exchange membrane fuel cells, J. Power sources 102 (2001) 82–96.
[32] G. Maggio, V. Recupero, L. Pino, Modelling polymer electrolyte fuel cells: an innovative approach, J. Power sources 101 (2001) 275–286.
[33] K.W. Lum, J.J. McGuirk, Three-dimensional model of a complete polymer electrolyte membrane fuel cell—model formulation, validation and parametric studies, J. Power Sources 143 (2005) 103–124.
[34] T.V. Nguyen, R.E. White, A water and heat management model for proton exchange membrane fuel cells, J. Electrochem. Soc. 140 (8) (1993) 2178–2186.
[35] J.S. Yi, T.V. Nguyen, An along-the-channel model for proton exchange membrane fuel cells, J. Electrochem. Soc. 145 (4) (1998) 1149–1159.
[36] V. Gurau, H.T. Liu, S. Kakac, Two-dimensional model for proton exchange membrane fuel cells, AIChE J. 44 (11) (1998) 2410–2422.
[37] A. Kazim, H.T. Liu, P. Forges, Modeling of performance of PEM fuel cells with conventional and interdigitated flow fields, J. Appl. Electrochem. 29 (1999) 1409–1416.
[38] D. Singh, D.M. Lu, N. Djilali, A two-dimensional analysis of mass transport in proton exchange membrane fuel cells, Int. J. Eng. Sci. 37 (1999) 431–452.

[39] W.S. He, J.S. Yi, T.V. Nguyen, Two-phase flow model of the cathode of PEM fuel cells using interdigitated flow fields, AIChE J. 46 (10) (2000) 2053–2064.
[40] Z.H. Wang, C.Y. Wang, K.S. Chen, Two-phase flow and transport in the air cathode of proton exchange membrane fuel cells, J. Power Sources 94 (2001) 40–50.
[41] D. Natarajan, T.V. Nguyen, A two-dimensional, two-phase, multicomponent, transient model for the cathode of a proton exchange membrane fuel cell using conventional gas distributors, J. Electrochem. Soc. 148 (12) (2001) A1324–A1335.
[42] I.M. Hsing, P. Futerko, Two-dimensional simulation of water transport in polymer electrolyte fuel cells, Chem. Eng. Sci. 55 (2000) 4209–4218.
[43] K. Dannenberg, P. Edkunge, G. Lindbergh, Mathematical model of the PEMFC, J. Appl. Electrochem. 30 (2000) 1377–1387.
[44] T.F. Fuller, J. Newman, Water and thermal management in solid-polymer-electrolyte fuel cells, J. Electrochem. Soc. 140 (5) (1993) 1218–1225.
[45] S. Dutta, S. Shimpalee, J.W. Van Zee, Three-dimensional numerical simulation of straight channel PEM fuel cells, J. Appl. Electrochem. 30 (2000) 135–146.
[46] S. Dutta, S. Shimpalee, J.W. Van Zee, Numerical prediction of mass-exchange between cathode and anode channels in a PEM fuel cell, Int. J. Heat Mass Transfer 44 (2001) 2029–2042.
[47] S. Shimpalee, S. Dutta, Numerical prediction of temperature distribution in PEM fuel cells, Numer. Heat Transfer, Part A 38 (2000) 111–128.
[48] T. Berning, D.M. Lu, N. Djilali, Three-dimensional computational analysis of transport phenomena in a PEM fuel cell, J. Power Source 106 (2002) 284–294.
[49] T. Berning, N. Djilali, Three-dimensional computational analysis of transport phenomena in a PEM fuel cell—a parametric study, J. Power Sources 124 (2003) 440–452.
[50] T.C. Jen, T. Yan, S.H. Chan, Chemical reacting transport phenomena in a PEM fuel cell, Int. J. Heat Transfer 46 (22) (2003) 4157–4168.
[51] P.W. Li, L. Schaefer, Q.M. Wang, T. Zhang, M.K. Chyu, Multi-gas transportation and electrochemical performance of a polymer electrolyte fuel cell with complex flow channels, J. Power Source 115 (2003) 90–100.
[52] G. Hu, J. Fan, S. Chen, Y. Liu, K. Cen, Three-dimensional numerical analysis of proton exchange membrane fuel cells (PEMFCs) with conventional and interdigitated flow fields, J. Power Sources 136 (2004) 1–9.
[53] S. Um, C.Y. Wang, Three-dimensional analysis of transport and electrochemical reactions in polymer electrolyte fuel cells, J. Power Sources 125 (2004) 40–51.
[54] P.T. Nguyen, T. Berning, N. Djilali, Computional model of a PEM fuel cell with serpentine gas flow channels, J. Power Sources 130 (2004) 149–157.
[55] T.H. Zhou, H.T. Liu, A 3D model for PEM fuel cells operated on reformate, J. Power Sources 138 (2004) 101–110.
[56] H. Ju, H. Meng, C.Y. Wang, A single-phase, non-isothermal model for PEM fuel cells, Int. J. Heat Mass Transfer 48 (2005) 1303–1315.
[57] A.A. Kulikovsky, Quasi three-dimensional modelling of the PEM fuel cell: comparison of the catalyst layers performance, Fuel Cells 1 (2) (2001) 162–169.
[58] P. Costamagna, Transport phenomena in polymeric membrane fuel cells, Chem. Eng. Sci. 56 (2001) 323–332.
[59] A. Bıyıkoğlu, Review of proton exchange membrane fuel cell models, Int. J. Hydrogen Energy 30 (2005) 1181–1212.
[60] N. Njilali, D. Lu, Influence of heat transfer on gas and water transport in fuel cells, Int. J. Therm. Sci. 41 (2002) 29–40.
[61] C. Ziegler, A. Schmitz, M. Tranitz, E. Fontes, J.O. Schumacher, Modeling planar and self-breathing fuel cells for use in electronic devices, J. Electrochim. Soc. 151 (12) (2004) A2028–A2041.
[62] H. Sun, H. Liu, L.J. Guo, PEM fuel cell performance and its two-phase mass transport, J. Power Sources 143 (2005) 125–135.
[63] S.H. Ge, B.L. Yi, A mathematical model for PEMFC in different flow modes, J. Power Sources 124 (2003) 1–11.
[64] L. Wang, A. Husar, T. Zhou, H. Liu, A parametric study of PEM fuel cell performances, Int. J. Hydrogen Energy 28 (2003) 1263–1272.
[65] L. Wang, H. Liu, Performance studies of PEM fuel cells with interdigitated flow fields, J. Power Sources 134 (2004) 185–196.
[66] M. Noponen, E. Birgersson, J. Ihonen, M. Vynnycky, A. Lundblad, G. Lindbergh, A two-phase non-isothermal PEFC model: theory and validation, Fuel Cells 4 (4) (2004) 365–377.
[67] M. Grujicic, K.M. Chittajallu, Optimization of the cathode geometry in polymer electrolyte membrane (PEM) fuel cells, Chem. Eng. Sci. 59 (2004) 5883–5895.
[68] G. Lin, W. He, T.V. Nguyen, Modeling liquid water effects in the gas diffusion and catalyst layers of the cathode of a PEM fuel cell, J. Electrochem. Soc. 151 (2) (2004) A1999–A2006.
[69] K.M. Yin, Parametric study of proton-exchange-membrane fuel cell cathode using an agglomerate model, J. Electrochem. Soc. 152 (3) (2005) A583–A593.
[70] L. Pisani, G. Murgia, M. Vlaentini, B. D'Aguanno, A working model of polymer electrolyte fuel cells comparisons between theory and experiments, J. Electorchem. Soc. 149 (7) (2002) A898–A904.
[71] D. Song, Q. Wang, Z. Liu, T. Navessin, S. Holdcroft, Numerical study of PEM fuel cell cathode with non-uniform catalyst layer, Electrochim. Acta 50 (2004) 731–737.
[72] M. De Francesco, E. Arato, Start-up analysis for automotive PEM fuel cell systems, J. Power Sources 108 (2002) 41–52.
[73] M. De Francesco, E. Arato, P. Costa, Transport phenomena in membranes for PEMFC applications: an analytical approach to the calculation of membrane resistance, J. Power Sources 132 (2004) 127–134.
[74] R. Roshandel, B. Farhanieh, E. Saievar-Iranizad, The effects of porosity distribution variation on PEM fuel cell performance, Renew. Energy 30 (2005) 1557–1572.
[75] B.R. Sivertsen, N. Djilali, CFD-based modeling of proton exchange membrane fuel cells, J. Power Sources 141 (2005) 65–78.
[76] S.H. Chan, S.K. Goh, S.P. Jiang, A mathematical model of polymer electrolyte fuel cell with anode CO kinetics, Electrochim. Acta 48 (2003) 1905–1919.
[77] P. Rama, R. Chen, R. Thring, A polymer electrolyte membrane fuel cell model with multi-species input, Proc. Inst. Mech. Eng., Part A: Power Energy 219 (4) (2005) 255–271.
[78] J.J. Baschuk, A.M. Rowe, X. Li, Modeling and simulation of PEM fuel cells with CO poisoning, Trans. ASME 125 (2003) 94–100.
[79] M. Eikerling, A.A. Kornyshev, Electrochemical impedance of the cathode catalyst layer in polymer electrolyte fuel cells, J. Electroanal. Chem. 475 (1999) 107–123.
[80] B. Carnes, N. Djilali, Systematic parameters estimation for PEM fuel cell models, J. Power Sources 144 (2005) 83–93.
[81] S. Mazumder, J.V. Cole, Rigorous 3-D mathematical modeling of PEM fuel cells. I. Model predictions without liquid water transport, J. Electrochim. Soc. 150 (11) (2003) A1503–A1509.
[82] S. Mazumder, J.V. Cole, Rigorous 3-D mathematical modeling of PEM fuel cells. II. Model predictions with liquid water transport, J. Electrochim. Soc. 150 (11) (2003) A1510–A1517.
[83] S. Um, C.Y. Wang, K.S. Chen, Computational fluid dynamics modeling of proton exchange membrane fuel cells, J. Electrochim. Soc. 147 (12) (2000) 4485–4493.
[84] S.M. Senn, D. Poulikakos, Polymer electrolyte fuel cells with porous materials fluid distributors and comparisons with traditional channeled systems, Trans. ASME 126 (6) (2004) 410–418.
[85] M. Hu, A. Gu, M. Wang, X. Zhu, L. Yu, Three dimensional, two phase mathematical model for PEM fuel cell. Part I. Model development, Energy Convers. Manage. 45 (2004) 1861–1882.
[86] M. Hu, A. Gu, X. Zhu, M. Wang, L. Yu, Three dimensional, two phase mathematical model for PEM fuel cell. Part II. Analysis and discussion of the internal transport mechanisms, Energy Convers. Manage. 45 (2004) 1883–1916.
[87] M.R. Hu, X.J. Zhu, A.Z. Gu, Simulation of the internal transport phenomena for PEM fuel cells with different modes of flow, Chin. J. Chem. Eng. 12 (1) (2004) 14–26.
[88] J.S. Yi, T.V. Nguyen, Multicomponent transport in porous electrodes of proton exchange membrane fuel cells using the interdigited gas distributors, J. Electrochem. Soc. 146 (1) (1999) 38–45.

[89] U. Pasaogullari, C.Y. Wang, Two-phase modeling and flooding prediction of polymer electrolyte fuel cells, J. Electrochem. Soc. 152 (2) (2005) A380–A390.
[90] F. Chen, Y.Z. Wen, H.S. Chu, W.M. Yan, C.Y. Soong, Convenient two-dimensional model for design of fuel channels for proton exchange membrane fuel cells, J. Power Sources 128 (2004) 125–134.
[91] H.S. Chu, C. Yeh, F. Chen, Effects of porosity change of gas diffuser on performance of proton exchange membrane fuel cell, J. Power Sources 123 (2003) 1–9.
[92] K.T. Jeng, S.F. Lee, G.F. Tsai, C.H. Wang, Oxygen mass transfer in PEM fuel cell gas diffusion layers, J. Power Sources 138 (2004) 41–50.
[93] H.K. Lee, J.H. Park, D.Y. Kim, T.H. Lee, A study on the characteristics of the diffusion layer thickness and porosity of the PEMFC, J. Power Sources 131 (2004) 200–206.
[94] K.W. Lum, J.J. McGurik, 2D and 3D modeling of a PEMFC cathode with interdigitated gas distributors, J. Electrochim. Soc. 152 (4) (2005) A811–A817.
[95] A. Kazim, P. Forges, H.T. Liu, Effects of cathode operating conditions on performance of a PEM fuel cell with interdigitated flow fields, Int. J. Energy Res. 27 (2003) 401–414.
[96] J.J. Hwang, C.K. Chen, R.F. Savinell, C.C. Liu, J. Wainright, A three-dimensional numerical simulation of the transport phenomena in the cathodic side of a PEMFC, J. Appl. Electrochem. 34 (2004) 217–224.
[97] X. Li, I. Sabir, Review of bipolar plates in PEM fuel cells: flow-field designs, Int. J. Hydrogen Energy 30 (2005) 359–371.
[98] H. Meng, C.Y. Wang, Electron transport in PEFCs, J. Electrochem. Soc. 151 (3) (2004) A358–A367.
[99] C.Y. Du, P.F. Shi, X.Q. Cheng, G.P. Yin, Effective protonic and electronic conductivity of the catalyst layers in proton exchange membrane fuel cells, Electrochem. Commun. 6 (2004) 435–440.
[100] S.H. Chan, W.A. Tun, Catalyst layer models for proton exchange membrane fuel cells, Chem. Eng. Technol. 24 (1) (2001) 51–57.
[101] W. Sun, B.A. Peppley, K. Karan, Modeling the influence of GDL and flow-field plate parameters on the reaction distribution in the PEMFC cathode catalyst layer, J. Power Sources 144 (2005) 42–53.
[102] J.J. Baschuk, X. Li, Modeling CO poisoning and O_2 bleeding in a PEM fuel cell anode, Int. J. Energy Res. 27 (2003) 1095–1116.
[103] G.A. Camara, E.A. Ticianelli, S. Mukerjee, S.J. Lee, J. McBreen, The CO poisoning mechanism of the hydrogen oxidation reaction in proton exchange membrane fuel cells, J. Electrochim. Soc. 149 (6) (2002) A748–A753.
[104] J. Zhang, T. Thampan, R. Datta, Influence of anode flow rate and cathode oxygen pressure on CO poisoning of the proton exchange membrane fuel cells, J. Electrochim. Soc. 149 (6) (2002) A763–A772.
[105] N. Wagner, E. Gülzow, Change of electrochemical impedance spectra (EIS) with time during CO-poisoning of the Pt-anode in a membrane fuel cell, J. Power Sources 127 (2004) 341–347.
[106] T. Mennola, M. Noponen, M. Aronniemi, T. Hottinen, M. Mikkola, M. Himanen, P. Lund, Mass transport in the cathode of a free-breathing polymer electrolyte membrane fuel cell, J. Appl. Electrochem. 33 (2003) 979–987.
[107] W. Ying, J. Ke, W.Y. Lee, T.H. Yang, C.S. Kim, Effects of cathode channel configurations on the performance of an air-breathing PEMFC, Int. J. Hydrogen Energy 30 (2005) 1351–1361.
[108] W. Ying, Y.J. Sohn, W.Y. Lee, J. Ke, C.S. Kim, Three-dimensional modeling and experimental investigation for an air-breathing polymer electrolyte membrane fuel cell (PEMFC), J. Power Sources 145 (2005) 563–571.
[109] W. Ying, T.H. Yang, W.Y. Lee, J. Ke, C.S. Kim, Three-dimensional analysis for effect of channel configuration on the performance of a small air-breathing proton exchange membrane fuel cell (PEMFC), J. Power Sources 145 (2005) 572–581.
[110] J.M. Stockie, K. Promislow, B.R. Wetton, A finite volume method for multicomponent gas transport in a porous fuel cell electrode, Int. J. Numer. Methods Fluids 41 (2003) 577–599.
[111] M. Grujicic, C.L. Zhao, K.M. Chittajallu, J.M. Ochterbeck, Cathode and interdigitated air distributor geometry optimization in polymer electrolyte membrane (PEM) fuel cells, Mater. Sci. Eng. B 108 (2004) 241–252.
[112] J.M. Corrêa, F.A. Farret, V.A. Popov, M.G. Simões, Sensitivity analysis of the modeling parameters used in simulation of proton exchange membrane fuel cells, IEEE Trans. Energy Convers. 20 (1) (2005) 211–218.
[113] C.H. Lee, H.B. Park, Y.M. Lee, R.D. Lee, Importance of proton conductivity measurement in polymer electrolyte membrane for fuel cell application, Ind. Eng. Chem. Res. 44 (20) (2005) 7617–7626.
[114] M. Saito, N. Arimura, K. Hayamizu, T. Okada, Mechanisms of ion and water transport in perfluorosulfonated ionomer membrane for fuel cells, J. Phys. Chem. B 108 (2004) 16064–16070.
[115] A. Parthasarathy, S. Srinivasan, A.J. Appleby, C.R. Martin, Temperature dependence of the electrode kinetics of oxygen reduction at the platinum/Nafion® interface—a microelectrode investigation, J. Electrochem. Soc. 139 (9) (1992) 2530–2537.
[116] L. Zhang, C. Ma, S. Mukerjee, Oxygen permeation studies on alternative proton exchange membranes designed for elevated temperature operation, Electrochim. Acta 48 (2003) 1845–1859.
[117] G.E. Suares, K.A. Hoo, Parameter estimation of a proton-exchange membrane fuel cell using voltage–current data, Chem. Eng. Sci. 55 (2000) 2237–2247.
[118] P. Berg, K. Promislow, J.St. Pierre, J. Stumper, Water management in PEM fuel cells, J. Electrochem. Soc. 151 (3) (2004) A341–A353.
[119] T. Thamapan, S. Malhotra, H. Tang, R. Datta, Modeling of conductive transport in proton-exchange membranes for fuel cells, J. Electrochem. Soc. 147 (9) (2000) 3242–3250.
[120] Q. Guo, V.A. Sethuraman, R.E. White, Parameter estimates for a PEMFC cathode, J. Electrochem. Soc. 151 (7) (2004) A983–A993.
[121] A. Hakenjos, K. Tüber, O. Schumacher, C. Hebling, Characterising PEM fuel cell performance using a current distribution measurement in comparison with a CFD model, Fuel Cells 4 (3) (2004) 185–189.
[122] H. Ju, C.Y. Wang, Experimental validation of a PEM fuel cell model by current distribution data, J. Electrochem. Soc. 151 (11) (2004) A1954–A1960.
[123] C.H. Min, Y.L. He, X.L. Liu, B.H. Yin, W. Jiang, W.Q. Tao, Parameter sensitivity examination and discussion of PEM fuel cell simulation model validation Part II: Results of sensitivity analysis and validation of the model, J. Power Sources 160 (2006) 374–385.
[124] L. You, H. Liu, A two-phase flow and transport model for the cathode of PEM fuel cells, Int. J. Heat Mass Transfer 45 (2002) 2277–2287.
[125] W.Q. Tao, Numerical Heat Transfer, 2nd ed., Xi'an Jiaotong University Press, Xi'an, 2001, 220.